Design of an Electromagnetic Actuator to couple Snap-Through Buckling

LZ Corrales
Mechanical and Aerospace Engineering
Cornell University
Ithaca, NY
lc965@cornell.edu

Jeffrey Kagle
Mechanical and Aerospace Engineering
Cornell University
Ithaca, NY
jak567@cornell.edu

***Abstract*—This paper presents a novel force-based haptic actuator that leverages snap-through instability to deliver compact, wearable indentation feedback. Addressing the limitations of existing indentation technologies—including bulkiness, inefficiency, slow response, or high-voltage operation—the work integrates a bistable snap-through beam with a custom-designed Lorentz-force solenoid actuator. A magnetic vector potential–based modeling framework is used to co-design the solenoid geometry and permanent-magnet plunger to meet the beam's force–displacement requirements while minimizing size, mass, and power consumption. Experimental validation of the solenoid force model demonstrates good agreement with measured data, and a fully integrated prototype achieves the required impulse force and displacement to reliably trigger snap-through and passive reset. The results establish snap-through instability, coupled with tailored electromagnetic actuation, as a viable and efficient mechanism for wearable force-based haptic feedback.**

***Index Terms*—Snap Through Buckling, Electromagnetic Actuator, Magnet Armature**

I. Introduction

Skin deformation and slip to is crucial for to provide haptic feedback and is easily produced by offering indentation and/or vibration stimuli on the skin. There are many force-based haptic actuators that deliver vibration, fewer that provide indentation, and from those indentation devices even fewer are capable of seamlessly integrating into wearables, the ultimate goal of this project to present a new method to provide indentation. Commonly used indentation feedback methods are limited in wearability. Pneumatic and fluid driven devices require bulky or tethered equipment for use, thermal-driven devices are slow and inefficient. Voltage-driven devices, typically dielectric elastomer actuators (DEAs), use high voltages providing low force and displacement output. Electromagnetic actuators (EMAs) if not customized off-the-shelf options such as voice coils (Lorentz force actuators) are heavy, prone to heating, and are inefficient since they are operating out of their intended purpose [1].

Acknowledging the limitations of these indentation actuators we explore an alternative actuation method called snap-through instability, a type of buckling that allows for a rapid shift of equilibrium states when a threshold force is reached. This mechanism can be found in Venus fly traps, clicking beetles [1] and hummingbirds among others. Man-made snapping structures are built with materials that possess a snap-though instability (snapping metamaterials), can exhibit a rapid release of energy, nonlinear energy modulation, and bistability [2]. Explored use cases include energy dissipation (deformable shock absorber structures), bimodal state applications (grippers, fluidics pumps), and movement (jumping robots) often deployed in soft robotics. Despite the strengths of snap-through instability, this technology has yet to be explored as a force-based haptic feedback actuator.

Previous work by the authors has focused on developing a portable, lightweight, low power snap-through beam structure designed to render tactile feedback. This device produces out-of-plane snap through by driving the ends of a beam together, inducing beam deformation to push against a flat surface until reaching a required threshold force to induce snap-through.

This beam structure lacks an actuator to complete the device. This paper focuses on the design and integration of an lorentz force actuator (solenoid) to provide the force and linear displacement required to induce snap-through after which the device naturally returns to its original configuration. As a proof of concept, this paper goes through a custom solenoid design for a predetermined beam structure.

The paper details relevant literature on designing solenoids and haptic feedback devices using solenoids (Relevant Literature), the requirements of the beam structure (Methods) the algorithm used to configure the solenoid design and the structural considerations of integration (Methods), lastly, testing the validity of the model with experimental data and detailing the final solenoid design (Results/Discussion).

II. Relevant Literature

- [3] Song and Lee present a miniaturized solenoid actuator with a permanent-magnet plunger specifically engineered to drive segmented robots capable of both linear and turning locomotion. The actuator consists of a wound electromagnetic coil surrounding an NdFeB permanent-magnet plunger, allowing actuation through controlled current. Unlike conventional spring-return solenoids, the use of a magnetic plunger increases force density and eliminates the need for passive restoring elements. The authors derive an analytical force model based on the Biot-Savart law, explicitly relating output force to solenoid geometry (length, inner/outer diameter), coil

turns, current, air gap, and magnetic remanence. This model is used to optimize actuator dimensions for miniaturized robotic segments, yielding a compact device (20 mm length, 1250 turns, 5 mm inner diameter) capable of generating approximately 0.6 N of force.
At the system level, the actuator design is deployed in paired configurations, where in-phase solenoid actuation produces rectilinear motion and out-of-phase actuation generates bending and turning. This pairing strategy allows a rigid, discrete actuator architecture to emulate peristaltic and serpentine behaviors typically associated with soft robots. Experimental validation demonstrates predictable scaling of force with coil turns and confirms the feasibility of using this solenoid in a two-segment robot. However, measured displacements fall below theoretical limits due to inter-segment slip and frictional losses, highlighting a key limitation of rigid solenoid actuation. Overall, the paper establishes a clear, physics-grounded design framework for solenoid-based actuators in segmented robots, prioritizing simplicity, scalability, and manufacturability over compliance or energy efficiency

- The paper "Integrated Analytical Modeling and Numerical Simulation Framework for Design Optimization of Electromagnetic Soft Actuators" [4] took an alternative approach to Song and Lee [3] and designed the magnetic plunger diameter and the coils simultaneously. Furthermore, Zolfaghari et. al approached optimization with the intention to scale into the millimeter range. The standard Bio-Savart law is a method to calculate a magnetic field at the center axis of wound coils often approximated to be the magnetic field across the entire cross-section of the coils. This assumption carries over into design requirements reducing the ability to optimize design parameters. This paper introduces a magnetic vector potential (MVP) approach derived from the Maxwell-Ampere law taking into account the spacial dependence of the coils magnetic field. The authors optimized with a Minimum Integer Non-Linear Program (MINLP) framework maximizing force over cross-sectional area to select magnet diameter and the number of turns per layer which is then extrapolated into the full solenoid geometry.
- [5] Flavin et al. introduces a miniaturized bio-elastic, bistable electromagnetic actuator that incorporates human skin as a functional mechanical element. The actuator consists of a solenoid like electromagnetic core, a permanent-magnet-based armature, and an elastomeric diaphragm, which together form a bistable system when coupled to the elastic response of skin. Mechanical energy stored in skin deformation stabilizes both compressed and relaxed states, enabling the actuator to maintain static indentation without continuous power input. State transitions are achieved by brief current pulses that either reinforce or counteract the permanent magnetic field, allowing controlled switching between states. This architecture yields large displacements (less than 2 mm) and forces (approx. 1.4 N) at markedly reduced energy cost relative to traditional electromagnetic, pneumatic, or electrostatic haptic actuators, while remaining compact and skin-conformable
The design supports multimodal operation through the same mechanical stack. Sub-threshold AC excitation enables vibrotactile actuation around either stable state, using the combined skin–diaphragm–armature system as a tunable spring–mass oscillator. The actuator is further extensible using modular contact interfaces, including a kirigami-based transmission that converts axial motion into controlled torsional shear at the skin surface. An integrated inductance-based self-sensing mechanism allows closed-loop control of armature position, compensating for inter- and intra-subject variability in skin mechanics and maximizing energy recovery during transitions. Collectively, these design choices position the actuator as a highly efficient, scalable building block for dense haptic arrays capable of delivering static, dynamic, and directional stimuli for sensory substitution and augmentation applications
- [6] Pece et al. presents the MagTics system that utilizes an array of magnetically actuated tactile pixels (taxels) in a flexible band to create a multi-functional and modular haptic feedback device. The paper addresses the limitations of conventional vibration-based haptics—namely low spatial resolution, bulky form factors, and high power consumption—by introducing bistable electromagnetic actuators arranged as taxels. These actuators can maintain force output without continuous power, enabling dense arrays suitable for flexible substrates.
One of the system's key technical contribution lies in its miniaturized, bistable solenoid-based actuation. By leveraging magnetic latching, each solenoid can switch states with brief current pulses and sustain tactile force without continuous power, significantly improving energy efficiency over conventional electromagnetic actuators. This solenoid architecture enables thin, high-density actuator arrays while mitigating heat and power constraints, representing an important advancement in how electromagnetic actuation can be adapted for flexible, wearable haptic systems.

III. Methodology

A. Selected Beam

For a starting point we selected a beam and actuator set up that works. The beam requires a 2.9N to trigger snap through from which the force requirement drops to around 1N around a third of its peak force. A horizontal displacement of 3.36mm is required to trigger snap through. At snap-though the vertical out-of-plane displacement of the beam is 4.3mm measured from the top of the structure holding the raised beam's end in place. The snap-through exerts a force of 1 - 2.5N depending on the total horizontal displacement of the beam's end when it's backing is grounded with the beam allowed to displace 4.3mm from the top of the beams casing.

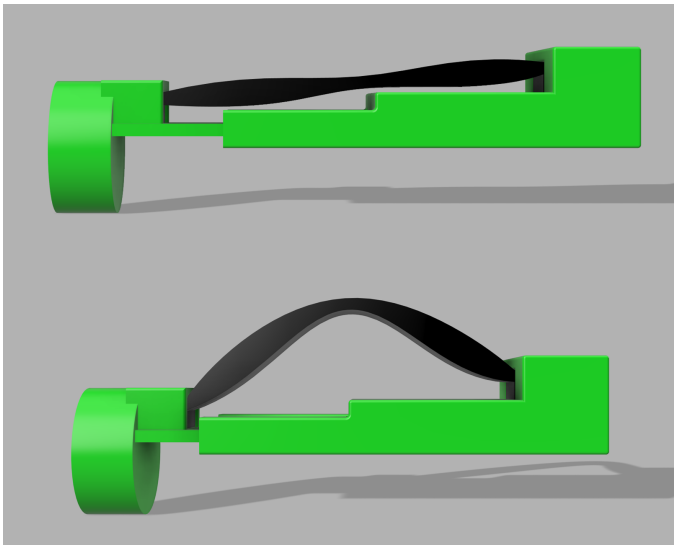


Fig. 1. Top: starting configuration of beam, Bottom: beam after snap through through linear displacement of one it's ends

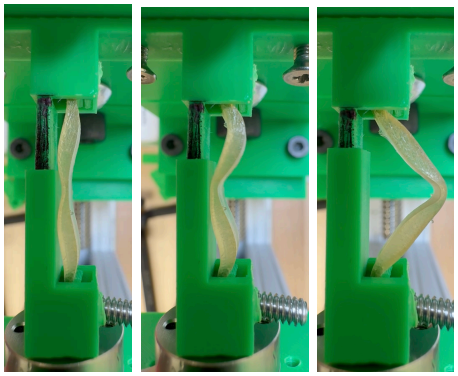


Fig. 2. Snap through beam in experimental setup. Left: no force applied, center: force applied but no snap, right: after snap occurs

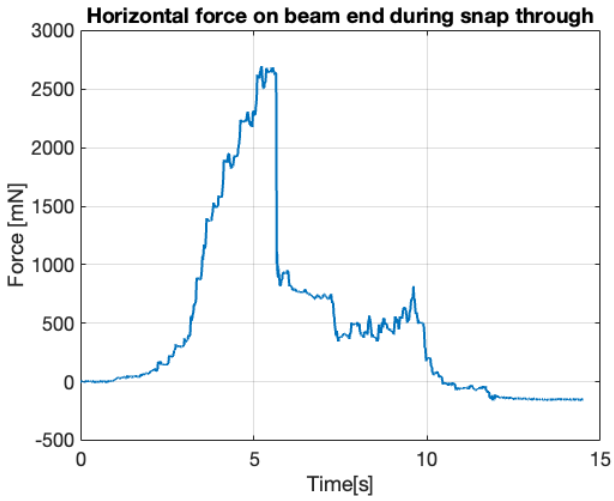


Fig. 3. Force over time of the selected snap-through beam structure see figure 2. At about 5.5 seconds is the release of energy from the snap-through of the beam.

An example of how the current snap-through beam design before and after actuation is shown in figure 1.

After the beam touches the force sensor any extra input force is transferred. However, the feeling of the beam on skin would vary as the skin experiences non-linear compression as does the beam. This interaction of the beam and skin is what makes this actuator unique.

The horizontal force to displacement profile of the beam (figure 2) demonstrates how when compressing the beam's end horizontally gradually increase force to a maximum where then it snaps-through to a smaller force where then no more horizontal displacement is possible. From here the release of the beam to it's original configuration exerts a much smaller force and even a snap back effect occurs. This release force can be used to passively reset a selected linear actuator.

B. Solenoid Design

In order to ensure snap-through for the beam setup described in section III-A the edge of the beam requires a 3.36mm linear displacement paired with a linear force reaching at least 2.9N. The selected actuator show take advantage of the beams force displacement properties. The nature of snap-through is a quick release of energy on the order of milliseconds, therefore only an impulse of power is required to snap-through. Once power is turned off and displacement is no longer required ideally, the beam's restoring force should reset the actuator as shown in figure 3. Moreover the linear actuator should be wearable translating to being compact, lightweight, and low power ideally to be powered untethered.

Electromagnetic actuators are well suited to furfill these requirements and are easily reconfigurable for variations of centimeter-sized beams and design goals. We selected a solenoid as our actuator based on it's ability to furfill the above requirements.

Off-the-shelf, commercial solenoids typically consist of an ferromagnetic armature (plunger) and coils housed in a casing. The addition of a spring between the plunger and casing can result in a pull or pull force and displacement output, likewise embedding magnets within the case can result in a latching configurations both additions depend on their placement within the solenoid.

To start off we tested a commercial solenoid rated at 12V, current draw around 0.25A, and 0.5N, and as expected, the force output could not horizontal displace the beam, see section III-C for more details about the setup.

A method to increase the force output of the solenoid without introducing more overall weight and volume, is to use a permanent magnet as the plunger. The use of a magnet as an plunger is not standard with commercially available solenoids, possibly due additional complication to the system from adding an additional magnetic field into the system. Therefore we determined the design parameters of a solenoid's coil and plunger to suit our current and future snap-through system.

Recently published work looked into simultaneously de-

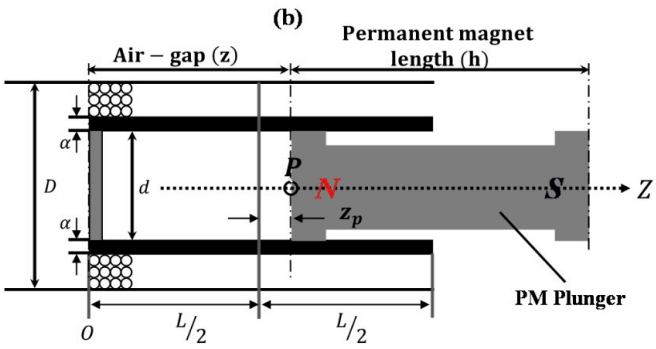


Fig. 4. Diagram of magnet inside a coil. From [3]

termining coil and magnet geometry using a magnet vector potential (MVP) approach derived from Maxwell-Amperé law in lieu of the traditional Bio-Savart approach. We employ the same MVP approach to determine to select parameters for our solenoid.

The force exerted on a permanent magnet with a coil present is computed by combining force exerted on the magnets north and south poles equation depicted in equation III-B as illustrated in figure 4. Where $F_{N,S}$ is the north and south pole respectively, B_r is the residual magnet flux density (for N52 magnets in 1.45 Tesla), r_m is the radius of the magnet, $\mu 0$ is the permeability of vacuum. The magnetic field of the current carrying coil, B_{coil}, is determined by summing up the contribution of each coil loop's magnetic field (Equation III-B) , $B_z(r, z, I)$. Where z and r are coordinates centered in the coil, l_{coil} is the length of the coil, and I is current. B_{coil} is the magnet field created by the current carrying coil.

$$F = F_N + F_S$$

$$F_{N,S} = \int_0^{r_m} \int_0^{2\pi} \frac{B_r}{\mu_0} B_{coilN,S} r dr d\phi$$

$$B_{coil} = \int_{-l_{coil}/2}^{l_{coil}/2} B_z(r, z, I) dz'$$

With the established force equation we can see how the force on the magnet changes when the its relative position to the coil changes (example demonstrated in figure 5). This is especially important to guarantee sufficient force and displacement.

In order to ensure an appropriate solenoid configuration, geometric and power parameters are swept within the MVP force model and the "best" configurations that meet the beam's snap-through requirements are are kept. The geometric and power parameters include the number of radial layers (Nl), number of axial turns per layer (Npl), wire diameter and magnet diameter (dm), the length of the magnet relative to the coil, residual magnet flux density of the magnet (Br), and the input current (I).The sweep range of each parameter is determined by application, thus ensuring only adequate configurations.

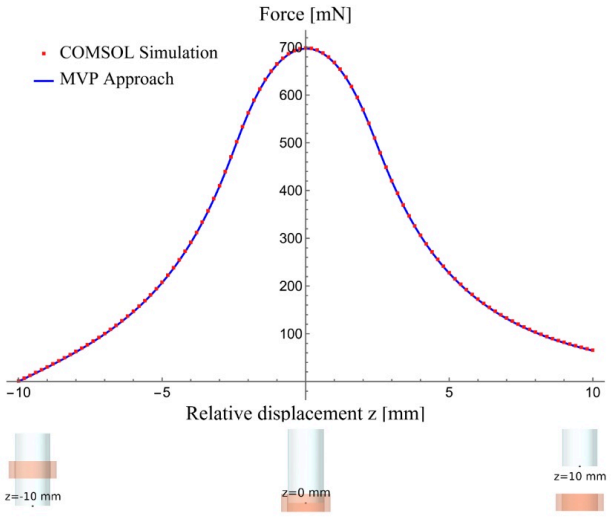


Fig. 5. Force exerted on the magnet from a current carrying coil. From [4]

For simplicity, the maximum force in the beam's force-displacement profile serves at the minimum force output of the solenoid over a "usable" displacement. The solenoids "usable" displacement is selected around the maximum of the force (see quadratic force profile in figure 5) to relative displacement of the coil and magnet profile. For simplicity, the "usable" displacement is selected to be 1/2 the length of the longer component (coil vs solenoid), where this component is covered within 1/4 to 3/4 of the other component.

C. Housing Structure Design

Our housing design consisted of four major components, organized into two subsystems. The first, the solenoid housing subsystem, included a solenoid base and a solenoid top. This subsystem ensured that the solenoid was fully enclosed while keeping its two leads accessible, maintained the alignment of the magnet beam, and incorporated a hard stop at the end of the beam to prevent it from falling out. The second subsystem was designed to hold the snap-through beam and included a snap beam head that moved along a snap beam rail, allowing motion in only one direction. In some iterations of the device, an additional support beam was also implemented to provide extra structural stability.

Our design was fabricated using 3D-printed PLA plastic, enabling rapid prototyping on a Bamboo Lab 3D printer. While this approach allowed for quick iteration, it introduced some challenges in controlling tolerances, as build orientation could affect surface finish and lead to slight expansion or compression of parts. To mitigate these issues, a minimum clearance of 0.1 mm was incorporated into all mating features, ensuring reliable assembly and proper fit between components.

During our iterations of the housing design, several considerations beyond tolerances became apparent. One significant design flaw occurred when the solenoid housing and snap-through beam housing were arranged in parallel rather than in series. This configuration introduced a bending moment in the

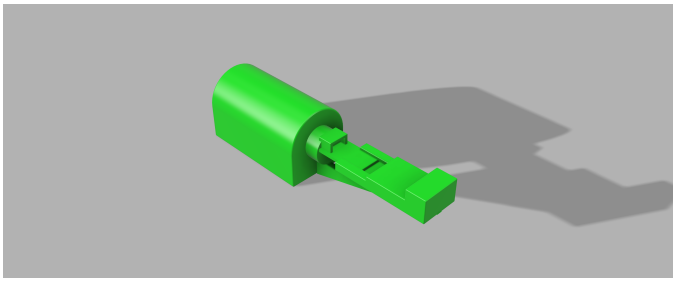


Fig. 6. Final Housing Design

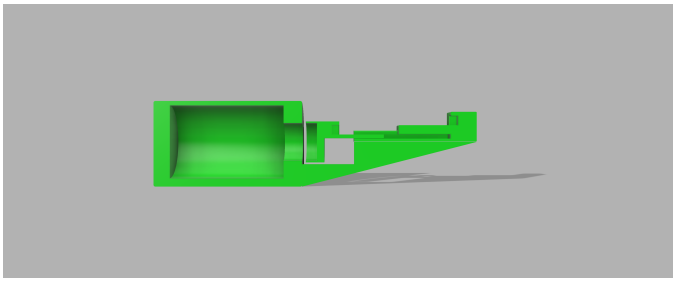


Fig. 7. Section View of Final Housing Design

beam, which significantly reduced the force transmitted from the solenoid to the snap-through beam. Another issue arose from the snap-through beam holder and rail, which initially did not fully constrain the beam's movement in all directions. Although this was not immediately apparent—since force was primarily applied in one direction—it exacerbated the bending moment and led to additional force loss. Furthermore, print orientation affected the surface finish of parts, which could increase friction in moving components if rough surfaces were produced, further impacting device performance.

IV. Results

A. Experimental Results of Solenoid Design Model

As a simple verification of the MVP model used to design solenoids, a commercial solenoid was tested. To gather force data We fixed the solenoid and attached the magnet to an ATI Nano force sensor, see setup in figure 8, and moved the magnet from the coil and magnet's edges aligned with the magnet to the having the other edge aligned again both with having the magnet fully outside if the coil. We modeled the solenoid based on the measured dimension of the commercial solenoid and an 1/4in diameter and 1/2in long N52 magnet (what was available in the lab). Figure 9 shows the plot of the model and experiment. Note that the overlaid experimental results x-axis is not properly aligned due to time constraints.

Model parameters were measured and computed as: 33 AWG, coil inner diameter = 8.8mm, coil outter diameter = 6.4mm, Number if axial layers = 10, number of turns per layer = 139, I = 0.25A, V = 12V, magnet air gap (between coil and magnet) = 1.2mm, magnet length = 1/27mm, magnet diameter 3.2mm.

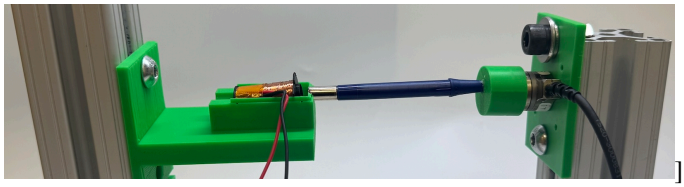


Fig. 8. Experimental setup of commercial solenoid and magnet

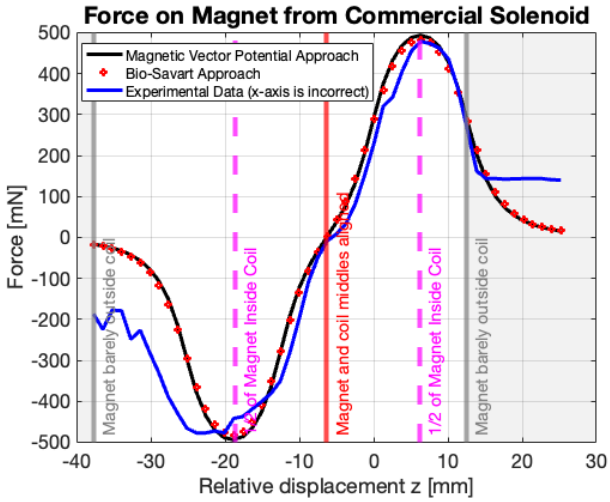


Fig. 9. Force-relative displacement of the coil and magnet from the setup shown in figure **??** with relative displacement established as is shown in figure 5.

Based on the selected beam a customized solenoid was designed based on prioritizing low power consumption (I) and ensuring the solenoid is small enough to not impede the feel of the beam. We use 30 AWG wire for allowable current use, air gap (between coil and magnet) of 0.2mm, set a maximum wire length of 100m, set the magnet length to match the length of the coil, and set the maximum coil thickness at 5mm to make the solenoid small enough for the system (Nl range restriction).

Sweep ranges are as follows: I: 0.3:0.1:0.5A, dm (magnet diameter) = (8:1:15)mm, Npl = 10:10:500; Nl = 15:1:20 The selected solenoid has the following parameters: I = 0.5A, dm = 10mm, Npl = 120, Nl = 18.

Resulting in the following metrics: Total wire length 85.22m, out coil diameter (do) = 19.5mm, total mass = 56.6 grams. Length of the coil and magnet = 30.5mm, thickness of coil = 4.6mm.

The force-relative displacement of the coil and magnet profile is shown in figure 10 with the highlighted blue region portraying the "usable" displacement region above the minimum required force.

V. Discussion

The commercial solenoid and magnet test to validate the MVP model with experimental data was successful. The maximum and minimum of each dataset is closely aligned. Since the experimental data does not reliably have the relative displacement data, we can qualitatively observe similar shapes

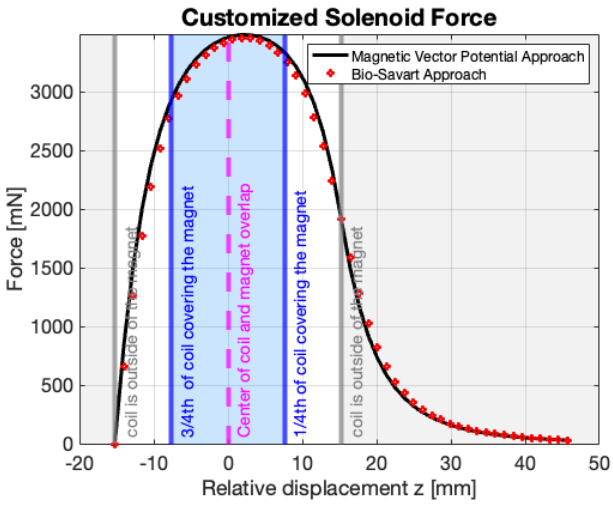


Fig. 10. Custom solenoid force-relative displacement of the coil and magnet profile with labeled positions. highlighted blue region portraying the "usable" displacement region above the minimum required force.

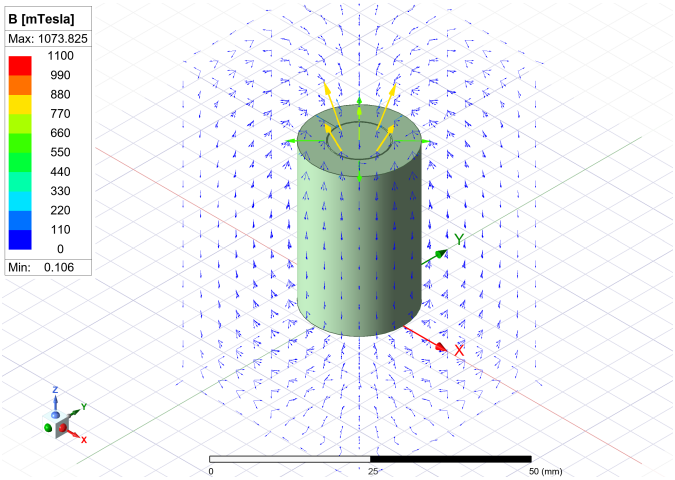


Fig. 11. B-vector field of solenoid

of their force profiles. Discrepancy occurs when the magnet is at the edge of the coil potentially due the imperfections of the magnet-coil alignment and edge coil winding.

The customized solenoid has a displacement has an excessively usable displacement range where the force is above the minimum required force ~19mm, where only 3.36mm was required. This is due to making the solenoid compact enough to work in series with the beam structure and using the maximum snap-through force requirement as the minimum force over the expected displacement length. The beam's force-displacement profile can be more closely aligned thus improving solenoid design parameters.

To determine how our ideal solenoid should act Ansys Maxwell simulations were completed to determine what our b-vector field (figure 11) and volume-force density of the coil (figure 12) and entire solenoid (figure 13) should be.

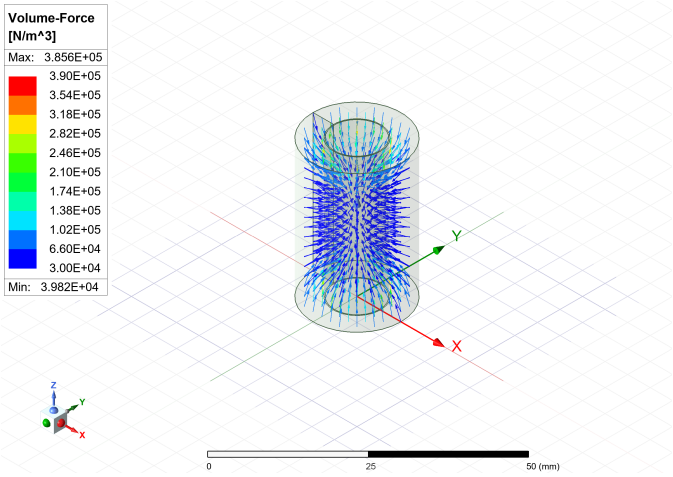


Fig. 12. Ideal volume-force density of coil

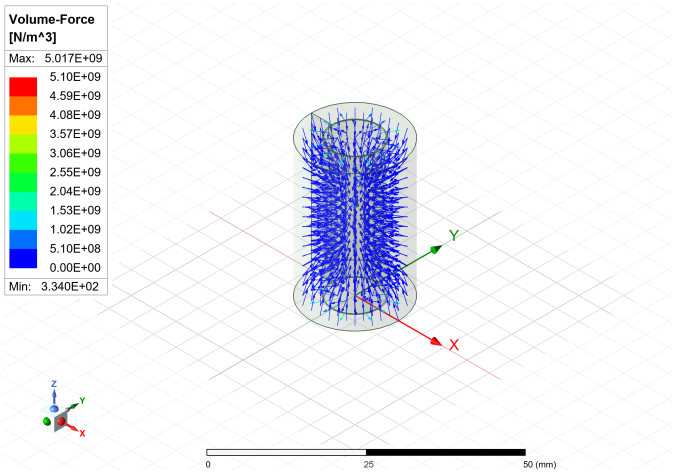


Fig. 13. Ideal volume-force density of solenoid

VI. Conclusions and Future Work

Next steps for actuator design is for more verification of the MVP model through experimental results. Additionally, there will be a focus on exploring the housing in which the coil and plunger placed for various geometric configurations of solenoids (disc shaped, longer plunger than coil, smaller coil than plunger). For example if the coil is lighter than the plunger than the plunger should move when powered and vise versa.

Future work will include taking advantage of the solenoids plunger force-displacement profile by closely aligning it to the beam's input force-displacement profile to reduce the weight and volume of the solenoid design.

Moreover, the overall snap-through force requirement is expected to improve through more exploration of the beam's design parameters, as such these this pipeline for geometric and power solenoid design will be useful as requirements shift.

The housing presented in this work was intended primarily as a test platform for characterizing the solenoid–snap-through beam system and enabling direct skin contact for

haptic perception experiments. Through iterative design, it was determined that optimal performance requires the solenoid and snap-through beam to be oriented in a linear configuration to minimize energy losses associated with bending moments and misalignment. Additionally, fully constraining the beam's motion to a single degree of freedom was found to be critical for efficient force transmission.

The proposed housing is not intended to be universally applicable. Instead, future implementations will require application-specific housings tailored to the designs form factor, load conditions, and environment. Potential future applications include integration into larger-scale haptic feedback devices, actuation of small jumping or impulse robotic systems, and use as a modular actuation element in a soft or hybrid robotic platform.

VII. Acknowledgments

Professor Elizabeth Farrell Helbling for mentoring and teaching. Thank you to Swecha Agarwal, Andrew Lin, Mehalin Desai, and Heather Jin Hee Kim. National Science Foundation for GRFP funds.

References

[1] Y. Wang, Q. Wang, M. Liu, Y. Qin, L. Cheng, O. Bolmin, M. Alleyne, A. Wissa, R. H. Baughman, D. Vella, and S. Tawfick, "Insect-scale jumping robots enabled by a dynamic buckling cascade," *Proceedings of the National Academy of Sciences of the United States of America*, vol. 120, no. 5, p. e2210651120, 2022. [Online]. Available: https://www.ncbi.nlm.nih.gov/pmc/articles/PMC9945960/

[2] S. Yan, L. Wu, Y. Wen, J. Sun, and J. Zhou, "Snap-through instability in mechanical metamaterials," *Responsive Materials*, vol. 3, no. 1, p. e20240035, 2025, _eprint: https://onlinelibrary.wiley.com/doi/pdf/10.1002/rpm.20240035. [Online]. Available: https://onlinelibrary.wiley.com/doi/abs/10.1002/rpm.20240035

[3] C.-W. Song and S.-Y. Lee, "Design of a Solenoid Actuator with a Magnetic Plunger for Miniaturized Segment Robots," *Applied Sciences*, vol. 5, pp. 595–607, Sep. 2015.

[4] H. Zolfaghari, N. Ebrahimi, Y. Ji, X. Pitkow, and M. Davoodi, "Integrated Analytical Modeling and Numerical Simulation Framework for Design Optimization of Electromagnetic Soft Actuators," *Actuators*, vol. 14, Mar. 2025.

[5] M. T. Flavin, K.-H. Ha, Z. Guo, S. Li, J.-T. Kim, T. Saxena, D. Simatos, F. Al-Najjar, Y. Mao, S. Bandapalli, C. Fan, D. Bai, Z. Zhang, Y. Zhang, E. Flavin, K. E. Madsen, Y. Huang, L. Emu, J. Zhao, J.-Y. Yoo, M. Park, J. Shin, A. G. Huang, H.-S. Shin, J. E. Colgate, Y. Huang, Z. Xie, H. Jiang, and J. A. Rogers, "Bioelastic state recovery for haptic sensory substitution," *Nature*, vol. 635, no. 8038, pp. 345–352, Nov. 2024, publisher: Nature Publishing Group. [Online]. Available: https://www.nature.com/articles/s41586-024-08155-9

[6] F. Pece, J. J. Zarate, V. Vechev, N. Besse, O. Gudozhnik, H. Shea, and O. Hilliges, "MagTics: Flexible and Thin Form Factor Magnetic Actuators for Dynamic and Wearable Haptic Feedback," in *Proceedings of the 30th Annual ACM Symposium on User Interface Software and Technology*, ser. UIST '17. New York, NY, USA: Association for Computing Machinery, Oct. 2017, pp. 143–154. [Online]. Available: https://doi.org/10.1145/3126594.3126609